

Article

Investigation of the Tunnel Water Inflow Prediction Method Based on the MODFLOW-DRAIN Module

Zhou Chen ^{1,*}, Zhaoqiang Su ^{1,†}, Mei Li ², Qi Shen ^{1,†}, Lufei Fan ² and Yanjie Zhang ^{2,*}¹ School of Earth Science and Engineering, Hohai University, Nanjing 210098, China² Dianzhong Water Diversion Co., Ltd., Kunming 650051, China

* Correspondence: chenzhoucly@hhu.edu.cn (Z.C.); yanjie_tm@163.com (Y.Z.);

Tel.: +86-13815418015 (Z.C.); +86-18184829789 (Y.Z.); Fax: +86-025-83787140 (Z.C.); +86-0871-65210000 (Y.Z.)

† These authors contributed equally to this work.

Abstract: The precise prediction of water inflow in tunnels is a key aspect of civil engineering. It is directly related to the progress of construction, the stability of caverns and the safety of construction personnel. Currently widely used calculation methods include the empirical formula method, the analytical method and the numerical simulation method. In situations where the geological conditions are complex and the boundary conditions are irregular, numerical simulation methods have clear advantages. However, there are still discussions about the rationality, accuracy and applicability of the definition of tunnel boundary conditions in numerical simulation methods. Based on the Groundwater Model System (GMS10.7) software, we investigate the feasibility of using the DRAIN module to describe tunnel boundaries and calculate water inflow. By comparing it with traditional empirical formulas, the feasibility of the method is verified, and the error is about 8%. In addition, this method is applied to predict the water inflow in the construction of an underground pumping station under complex geological conditions and the prediction is compared with the measured water inflow, and the error is about 20%. This article explains the physical meaning and the value method of the relevant parameters of the DRAIN module, providing basic support for the prediction of water inflow in tunnels.

Keywords: water inflow; numerical simulation; DRAIN module; complex geological condition

Citation: Chen, Z.; Su, Z.; Li, M.; Shen, Q.; Fan, L.; Zhang, Y. Investigation of the Tunnel Water Inflow Prediction Method Based on the MODFLOW-DRAIN Module. *Water* **2024**, *16*, 1078. <https://doi.org/10.3390/w16081078>

Academic Editor: Giuseppe Pezzinga

Received: 13 March 2024

Revised: 6 April 2024

Accepted: 8 April 2024

Published: 10 April 2024



Copyright: © 2024 by the authors. Licensee MDPI, Basel, Switzerland. This article is an open access article distributed under the terms and conditions of the Creative Commons Attribution (CC BY) license (<https://creativecommons.org/licenses/by/4.0/>).

1. Introduction

Water conservancy, transportation, underground mineral mining and other types of projects all involve tunnel excavation and may cause sudden water surges. Surging water can cause a series of adverse effects, such as tunnel destabilization, casualties, construction schedule delays, ground settlement and environmental degradation. Grouting is usually used to improve the strength of rock masses around a tunnel, and it has an effect in preventing water disaster [1]. Research on the calculation and prediction of water inflow in tunnels is of great significance for tunnel safety, water resource protection and environmental protection.

Underground water-bearing formations often feature intricate cavities, exhibiting marked heterogeneity and anisotropy. The groundwater within these formations demonstrates complex movement patterns, influenced by factors like backfill, diameter and discharge rates. Prior to tunnel excavation, the primary pathways for groundwater flow are pores, fissures and channels shaped by long-standing geological and hydrological processes. Post-excitation, the tunnel itself transforms into a principal channel for groundwater discharge.

There are many methods for calculating and predicting water inflow, which can mainly be divided into the following categories: The empirical formula method [2,3] is usually derived from the summary of engineering practice and has good prediction accuracy in calculating water inflow problems under simple geological conditions. The traditional

empirical formula only considers a few individual parameters in the calculation, such as the initial groundwater level, the geometric size of the tunnel and the permeability coefficient of the rock mass, and ignores other influencing factors, such as rock type, precipitation and cracks. In addition, the traditional empirical formula treats an aquifer as a homogeneous and isotropic medium. This assumption cannot be applied to fractured rock masses, which leads to a certain deviation between the water inflows calculated with the empirical formula and the actual technique. The analytical formula method can be divided into the mirror method [4,5], the shaft method [6,7], the conformal transformation method [5,8,9] and other methods [10–13]. This type of method has a rigorous theoretical derivation, a simple calculation process and is suitable for engineering applications. However, each analytical method makes certain assumptions and cannot be applied to all engineering applications. This also leads to certain deviations between the calculation results and the technical reality.

Numerical simulation methods are an important tool for the quantitative analysis and calculation of groundwater and are particularly suitable for complex geological conditions and irregular boundary conditions. Many scientists have used numerical methods to calculate and analyze the intrusion of tunnel water under different geological conditions. Shi [14] proposed two pooled regression methods (PRB and PRF) based on polynomial regression and decision trees. The two proposed ensemble regression methods produce more accurate prediction results, and the PRF method performs best in most experiments. Dai [15] has presented a three-dimensional numerical model based on the smoothed particle hydrodynamics (SPH) method and validated it for two underwater landslides. Tisler et al. [16] conducted numerical simulations to investigate the differences between the Richards equation and the two-phase flow model, using an in-house code based on the finite volume method. Guo et al. [17] successfully addressed the exact analytical solution of the seepage field for multiple underwater tunnel problems for the first time, using the Schwartz alternating method combined with conformal mapping, taking into account arbitrary tunnel arrangements and tunnel interaction. Zhang et al. [18] utilized a dual permeability model to calculate the water inflow into tunnels and the anisotropic flow behavior with finite element numerical simulations. The results demonstrate that the dual permeability model can provide accurate predictions for the Huang Jiagou Tunnel and describe the anisotropic flow behavior in stratified rock mass tunnels.

Further advancements in this field have been made by Zhao et al. [19], who investigated the characteristics of water inflow in tunnels within a fault fracture zone. A model test was conducted to explore the influence of surface water and the effect of grouting on the water pressure distribution and inflow quantity in tunnels. Based on monitoring of inflow quantity, there are four stages: wet stages, dripping stages, gushing stages and collapse stages. Ref. [20] utilized the MODFLOW(2005)-USG method to study the groundwater flow model of the middle reaches of the Heihe Basin. The accuracy of the simulation results in the focused zone near the river was improved by generating a finer unstructured grid for the irregular and variously sized river boundary. Ju et al. [21] developed an integrated model (MODFLOW(2000)-ANN) by combining the merits of the numerical groundwater flow model MODFLOW and the artificial neural network model (ANN). This model improved the predictive accuracy and was successfully applied to modeling the spring discharge dynamic. WANG et al. [22] introduced the characteristics and the theoretical basis of the design of Visual MODFLOW in their paper and also discussed some problems and suggestions regarding its applications. Xia [23] conducted four groups of numerical experiments with different scales of grid cells to analyze the error characteristics in well flow simulation using MODFLOW. By comparing the numerical results with the analytical solutions derived from Theis's Equation, Xia identified three types of errors: solution errors, interpolation errors and depiction errors. A solution error is attributed to the MODFLOW core program, while an interpolation error arises from estimating the head distribution between adjacent cell centers.

This field continues to evolve with contributions from researchers who have expanded the application of numerical simulation in groundwater analysis. Reimann, T [24] in-

roduced the hybrid model MODFLOW(2005) Conduit Flow Processes (CFP), designed to compute groundwater flow processes within karst aquifers by coupling a continuum representing the low conductive matrix with a discrete pipe network. Zhang et al. [25] integrated a simple overland flow module (isochronous cells model) with the river module of MODFLOW, allowing for the simulation of temporal and spatial interactions between stream flow and groundwater using net rainfall data for a watershed. Cheng et al. [26] presented the application of GMS to accelerate the detailed modeling of the groundwater flow system in the North China Plain. Zhao et al. [27] used MODFLOW to simulate the current field in sliding mass to enhance understanding of landslide formation and provide a foundation for landslide control. Raheem, A et al. [28] investigated the impact of various groundwater extraction scenarios on water table fluctuations within the Lower Bari Doab Canal command area, using crop water demand assessments and MODFLOW modeling to inform sustainable agricultural and groundwater management practices. Sanaullah, M et al. [29] utilized Visual MODFLOW(2000) to evaluate the water balance of the Rechna Doab aquifer in Pakistan, highlighting the significant role of irrigation and rainfall in groundwater recharge and proposing canal lining and tube well installation as effective measures for reducing seepage and reclaiming water-logged land for agriculture. Rubio-Arellano, AB et al. [30] introduced a hydrodynamic model to simulate the behavior of the Celaya Valley aquifer in Mexico, accurately forecasting its response under different scenarios and underscoring the importance of continued water conservation and monitoring efforts. Li et al. [31] employed this software for groundwater resource assessment in the Longxi area of Daqing City, conducting simulation and prediction of groundwater. Diaz et al. [32] aimed to develop a methodology for representing the analytical hyporheic flux equation model (AHF) in a numerical model performed in MODFLOW. Ostad, H et al. [33] investigated the effects of karst conduit patterns on spring hydrographs, finding that conduit configuration and density, along with recharge type, significantly influence hydrograph characteristics such as peak discharge and recession rates. Hunt, M [34] proposed a conceptual model approach using MODFLOW-6 to address the complexities of managing the Estonia–Latvia transboundary aquifer, stressing the need for cross-border collaboration and adherence to international agreements for sustainable management. Xu et al. [35] developed the program package PRD (Planar Recharge and Discharge Package) based on the subroutine RCH (Recharge Package) to address the lack of planar flux simulation in MODFLOW, allowing area recharge or discharge in all layers with varying values. Wei et al. [36] introduced the potential of the Visual MODFLOW model and its application in studying hydrogeological conditions in sandstone-type uranium deposits. Cheng [37] conducted a series of simulation tests on a typical hydrogeological model to analyze the impacts of different solution methods and parameter combinations in MODFLOW. Dong Pei [38] discussed the reliability of using MODFLOW to simulate the seepage of free surfaces to overcome deficiencies of physical simulation and analytical methods. Ma et al. [39] applied Visual MODFLOW to model the trajectories of underground water particles in an opencast mine. Their findings contribute to decision-making processes by predicting changes in water levels and quality, thereby providing a solid foundation for the selection of appropriate monitoring systems and protective measures. Shu et al. [40] developed the MODFLOW(2005)-Gslib software based on MODFLOW, addressing uncertainties in groundwater modeling by combining hydrogeological parameter uncertainty research with geostatistical developments. Qin et al. [41] introduced an innovative approach by integrating MODFLOW with an artificial neural network, significantly enhancing the prediction of spring flow based on distinctive spring characteristics. This model serves as a vital tool for guiding groundwater exploitation strategies in karst regions, offering precise references for managing spring catchments. Liu et al. [42] developed a numerical model based on MODFLOW for saturated-zone groundwater flow and radionuclide transport in a research area to evaluate migration trends and environmental impacts.

When using the DRAIN package to calculate tunnel inflows, there are a number of value problems, such as difficulty in determining the conduction parameter [43,44]. When

simulating with DRAIN, the drainage coefficient (C) is mostly taken as an empirical value or inverted by using a cave section where gushing water has already occurred [45,46]. However, in order to clarify the physical meaning of the corresponding parameters in the drainage ditch under tunnel construction conditions, the value method for each parameter is not yet clear. In this paper, the physical significance of the parameters in the DRAIN module is thoroughly investigated and explained, and improvements are proposed for the previous methods of using empirical values or inverting the parameter values through specific conditions. Therefore, this article is based on the Groundwater Model System (GMS) simulation software and attempts to clarify the physical meaning and value methods of the relevant parameters of the drainage module. After comparing and discussing the empirical formula method, it becomes clear that the DRAIN module is suitable for describing tunnel boundaries and calculating water inflow. The applicability of this method in practice is also discussed.

2. Theoretical Research

There are several numerical methods for dealing with tunnel boundary conditions: constant water columns, drainage ditches, flow and the equivalent permeability coefficient. Drainage ditches discharge groundwater from an aquifer. The discharge volume is proportional to the difference between the water column in the aquifer (h) and the water column in the trench (h_D). If the water column in the aquifer is lower than the water column in the trench, the discharge volume is zero. This submodule can only discharge water and does not allow any flow to the aquifer. Therefore, this module can be used to calculate the karst pipe flow according to the hydraulic exchange characteristics between the trench submodule and the aquifer. Formulas (1) and (2) [47] are used in the model to calculate the flow exchange volume between the aquifer and the karst pipes:

$$Q_D = C_D(h - h_D), h > h_D \quad (1)$$

$$Q_D = 0, h \leq h_D \quad (2)$$

where Q_D is the discharge volume of the karst pipeline; C_D is the equivalent hydraulic conductivity coefficient, which is related to the shape of the converging water flow in the pipeline and the properties of the pipeline; h is the water column of the aquifer; and h_D represents the water head in the pipeline.

The purpose of developing the river submodule in MODFLOW is to simulate the flow between surface water and groundwater. Whether a river recharges or discharges groundwater depends on the hydraulic gradient between the river unit and the groundwater of the adjacent units. If the groundwater head (h) is greater than the river head (h_R), the groundwater adds water to the river; if the groundwater head is less than the river head, the river adds water to the groundwater. Therefore, this module can be used to calculate the karst pipe flow according to the hydraulic exchange characteristics between the flow submodule and the aquifer. Formulas (3) and (4) [47] are used in the model to calculate the exchange volume between the aquifer and the karst pipes.

$$Q_R = C_R(h_R - h), h > h_{BOT} \quad (3)$$

$$Q_R = C_R(h_R - h_{BOT}), h \leq h_{BOT} \quad (4)$$

where Q_R is the flow rate between the karst pipeline and the aquifer; C_R stands for the hydraulic conductivity coefficient of the connection between the pipeline and the aquifer; h stands for the water column of the aquifer; h_R is the water column of the karst pipeline; and h_{BOT} stands for the bottom head of the karst pipeline. If the head of the aquifer (h) is equal to the head of the pipeline (h_R), the flow rate is zero. If the head of the aquifer increases, the flow rate assumes a negative value, which means that groundwater flows into the pipeline; if the head of the aquifer decreases, the flow rate assumes a positive value,

i.e., the pipeline water flows into the aquifer. Before h reaches the value h_{BOT} , Q_R increases linearly as h decreases, and then the flow rate remains constant.

The traditional empirical formula only considers a few individual parameters in the calculation, such as the initial groundwater level, the geometric size of the tunnel and the permeability coefficient of the rock mass, and ignores other influencing factors, such as rock type, precipitation and cracks. Furthermore, the traditional empirical formula treats the aquifer as a homogeneous and isotropic medium. This assumption cannot be applied to fractured rock masses, which leads to a certain deviation between the water inflows calculated with the empirical formula and the actual technique. These empirical (Table 1) formulas apply under the following conditions.

Table 1. Commonly used empirical formulas.

	Expression	Symbolic Meaning
Joubouyi’s formula [48]	$Q = 1.366K \frac{(2H-S)S}{\lg R - \lg r}$	Q is the well water inflow (m^3/d); K is the permeability coefficient of the phreatic aquifer (m/d); H is the thickness of the phreatic layer (m); S is the stable water level drop in the well (m); R is the radius of the funnel when stable (m); r is the radius of the well (m).
Kuniaki Sato’s formula [49]	$Q_{max} = \frac{2\pi mKH_0L}{\ln \left[\tan \frac{\pi(2H_0-r)}{4hc} \cot \frac{\pi r}{4H} \right]}$ $Q = Q_{max} - 0.584\varepsilon \cdot K \cdot r$	Q_{max} is the predicted maximum possible water inflow through the tunnel (m^3/d); Q is the predicted stable water inflow through the tunnel (m^3/d); K is the permeability coefficient of the rock mass (m/d); H_0 is the static water level to the center of the equivalent circle of the tunnel cross-section distance (m); L is the length of the tunnel passing through the aquifer (m); r is the equivalent circle radius of the tunnel cross-section (m); H is the thickness of the water-bearing body (m); ε is the test coefficient (generally 12.8).
Kosgakov’s formula [49]	$Q_s = \frac{2\alpha KH_0L}{\ln R - \ln r}$ $\alpha = \frac{\pi}{2} + \frac{H_0}{R}$	Q_s is the predicted stable water inflow of the tunnel (m^3/d); K is the rock mass permeability coefficient (m/d); H_0 is the distance from the static water level to the center of the equivalent circle of the tunnel cross-section (m); L is the length of the tunnel passing through the aquifer (m); r is the equivalent circle radius of the tunnel cross-section (m); R is the radius of influence of tunnel water inrush.

In the ideal model, the study area is generalized to a homogeneous isotropic three-dimensional equivalent continuum model and the steady-state flow analysis method is used for the calculation. Therefore, the mathematical model of steady-state groundwater flow is chosen in this article:

$$\begin{cases} \frac{\partial}{\partial x} \left(K_x \frac{\partial H}{\partial x} \right) + \frac{\partial}{\partial y} \left(K_y \frac{\partial H}{\partial y} \right) + \frac{\partial}{\partial z} \left(K_z \frac{\partial H}{\partial z} \right) + \varepsilon = S_s H & (x, y, z) \in \Omega \\ H(x, y, z) = H_\Gamma(x, y, z) & (x, y, z) \in \Gamma_1 \\ K_x \frac{\partial H}{\partial x} + K_y \frac{\partial H}{\partial y} + K_z \frac{\partial H}{\partial z} = q_0(x, y, z) & (x, y, z) \in \Gamma_2 \end{cases} \quad (5)$$

where H is the groundwater head (m); K_x , K_y and K_z are anisotropic main permeability coefficients (m/d); “ ε ” is the source and sink term strength ($1/d$); S_s is the water storage rate ($1/m$); Ω is the seepage area; Γ_1 is the first boundary type of the study area, the constant head boundary; Γ_2 is the second boundary type of the study area, the constant flow boundary; $H_\Gamma(x, y, z)$ is the first type of boundary condition (m); and $q_0(x, y, z)$ is the second type of boundary unit area through water section recharge flow (m^2/d).

The MODFLOW(2000) software package for dewatering trenches was developed to simulate the effects of features such as tunnel excavations. As long as the water column in the aquifer is above a certain fixed water column or head (known as the outflow head), the outflow trench behaves in the same way as the aquifer. The difference in the hydraulic head is proportional to the rate at which water is discharged from the aquifer. This module can only discharge water and cannot allow water to flow into the aquifer. As long as the water column of the aquifer is above this height, the module drains the water from the aquifer at a rate that is proportional to the difference between the water column of the aquifer and a certain height (the so-called discharge height). However, if the water column of the aquifer

is lower than the height of the discharge, the discharge has no effect on the aquifer. This proportionality constant (C) is referred to as the conductivity of the channel.

$$\begin{aligned} Q_{out} &= C(h_{i,j,k} - H_D), h_{i,j,k} > H_D \\ Q_{out} &= 0, h_{i,j,k} \leq H_D \end{aligned} \quad (6)$$

where Q_{out} is the flow rate from the aquifer into the drainage ditch (m^3/d), C is the drainage coefficient (m^2/d), H_D is the DRAIN elevation (m) and $h_{i,j,k}$ is the water head (m) in DRAIN.

The coefficient C in Equation (6) is a superposition (or equivalent) discharge coefficient that describes all pressure losses between the discharge outlet and the area of units i, j and k , where the pressure head ($h_{i,j,k}$) can be assumed to be dominant. C is influenced by the flow behavior of the water into the drainage system and is related to the drainage system and the environment. It depends on the design of the drainage system (e.g., the size and shape of the drainage pipe) and the permeability properties in the vicinity of the drainage pipe.

Based on Darcy's law, the flow (Q_{out}) can be expressed as follows:

$$Q_{out} = K \cdot A \cdot \frac{h_{i,j,k} - HD}{L} \quad (7)$$

where K is the permeability coefficient of the medium, A is the total cross-sectional area of DRAIN (m^2) and L is the distance the water flows.

Based on Formulas (6) and (7), the following equation can be derived as follows:

$$C = \frac{K \cdot A}{L} \quad (8)$$

when calculating the water inflow into the tunnel, the tunnel excavation forms a series of fault zones that increase the permeability of the rock near the tunnel, i.e., increase K , while the rock further away remains essentially unaffected. Therefore, the value of C is mainly influenced by the fault zone of the tunnel excavation. In this article, the influence of the distant rock on the dewatering coefficient (C) is ignored and only the influence of the fault zone of the tunnel excavation is considered. Therefore, L is the thickness of the fault zone formed after tunnel excavation. This thickness is assumed to be two times the effective circular radius of the tunnel section.

$$C = \frac{K \cdot A}{l} \quad (9)$$

In the following chart, l is the thickness of the fault zone that forms after tunnelling and is twice the equivalent circular radius of the tunnel cross-section in meters. A schematic diagram is shown in Figure 1.

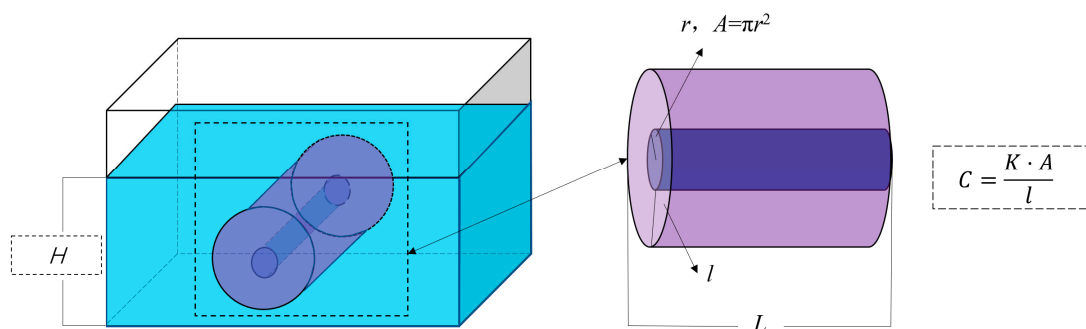


Figure 1. Schematic diagram of tunnel excavation section.

Next, this article will utilize GMS to establish a MODFLOW model. We will apply a specific value method to calculate the parameter C for the tunnel. This involves comparing the predicted water inflow with the actual water inflow observed during tunnel excavation. The aim is to verify the rationality of the adjusted value method. The specific flow chart is shown in Figure 2.

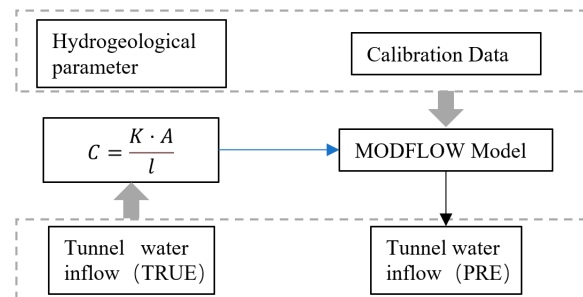


Figure 2. C—Schematic diagram of rationality verification process.

3. Case Analysis

3.1. Study Settings

The accuracy of numerical calculations is influenced by factors such as the model domain, the boundary conditions and the material parameters. We selected a specific model domain and boundary configurations based on their relevance to the typical conditions encountered in underground tunnel projects. A small distance between the tunnel boundary and the model's outer boundary leads to an overestimation of water inflow in the tunnel. Conversely, a large distance extends the calculation time and complicates post-processing.

We used a quadratic model spanning 2000 m for our calculations. The aquifer was assumed to be isotropic, with a thickness (H) of 150 m. The boundary condition was set to a constant water column of 150 m. This particular geometry and boundary condition were chosen to simulate realistic conditions accurately while ensuring computational efficiency. At the study area's center, a tunnel extends 300 m in length, positioned 75 m deep, covering an area of 600 m². The model's grid measures 20 m × 20 m × 30 m across 50,000 grids. The east–west boundary maintains a constant water column of 150 m, while the north–south boundary is watertight. A three-dimensional diagram of the model is shown in Figure 3. The middle part of the model is the location of the tunnel. The tunnel's length, being shorter than the model's, minimizes boundary effects on the calculations.

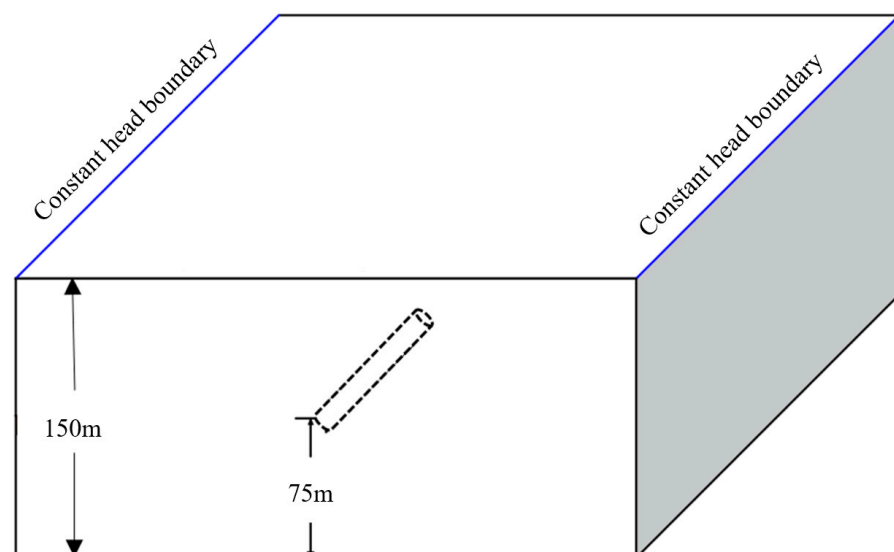


Figure 3. Three-dimensional schematic diagram of the study model.

To align the model setup closely with empirical equation assumptions, we set the east–west boundary as a fixed-head boundary with a head value of 150 m. The north–south boundary was designated a no-flow boundary.

This simulation considered two primary factors: the tunnel length-to-investigation area ratio and the rock’s permeability coefficient. We adjusted the tunnel length to modify the length-to-area ratio. Given that water ingress in tunnels typically happens in limestone layers with high permeability, we limited the rock’s permeability coefficient to a range of 0.1–0.3 m/d in our study.

Excavating tunnels below the water table changes the seepage field around the rock. Ignoring analysis of this factor can lead to geological disasters from excessive water inflow. Although determining the rock’s permeability parameters is challenging, it is critical for understanding the seepage field distribution and seepage water stability in the construction area. The rock’s permeability coefficient directly influences the seepage field distribution and the accuracy of its calculations. It is essential for tunnel structure design and analysis. Therefore, accurately identifying the permeability coefficient in the construction area is key to ensuring safe construction, reliable operation and the project’s overall success.

3.2. Calculation Results

Altering the tunnel length and the rock layer’s permeability coefficient resulted in varying simulation outcomes. The results of the simulation calculations are shown in Table 2. After tunnel excavation, the permeability coefficient of the surrounding rock after tunnel excavation is slightly greater than K . The empirical formula considers the initial groundwater level and certain parameters like tunnel geometry and rock mass permeability. However, it overlooks factors like rock type, water supply, precipitation and crack opening. This leads to minor discrepancies from the actual technical conditions.

Table 2. Calculation results.

K	L = 220 m		L = 200 m		L = 180 m		L = 160 m	
	EMP	SIM	EMP	SIM	EMP	SIM	EMP	SIM
0.1	1303.20	1102.88	1184.72	1056.00	1066.25	1008.53	1066.25	1008.53
0.15	1787.12	1593.20	1624.66	1528.09	1462.19	1457.18	1462.19	1457.18
0.2	2259.82	2083.81	2054.38	1992.25	1848.94	1902.92	1848.94	1902.92
0.25	2724.69	2565.66	2476.99	2457.81	2229.29	2343.59	2229.29	2343.59
0.3	3183.63	3050.79	2894.21	2921.75	2604.79	2789.36	2604.79	2789.36

3.3. Discussion

The comparison of water inflow estimates—from the empirical average formula and numerical simulation shown in Figure 4—reveals a notable accuracy. Specifically, when the tunnel length (L) is 220 m and 200 m, corresponding to tunnel length-to-study area ratios of 1:9 and 1:10, and with a permeability coefficient (K) of 0.2–0.3 m/d, the discrepancy in the average water inflow calculations is minimal, around 3%. In cases where L is 180 m and 160 m, equating to ratios of 1:11 and 1:12, respectively, with the same range of K , the error margin further decreases to about 2%.

When the tunnel length-to-study area ratio exceeds 1:9, water inflow estimates from the empirical method fall below those from numerical simulations. Conversely, if this ratio is under 1:12, the empirical method predicts higher water inflow than numerical simulations. Analysis of curve trends in the figure indicates that both methods’ water inflow predictions decrease as the tunnel length-to-study area ratio diminishes, assuming this ratio remains constant.

Holding the permeability coefficient steady, Figure 5 illustrates that with tunnel lengths of 200 m and 180 m (ratios of 1:10 and 1:11, respectively), the discrepancy in average water inflow calculations between the empirical and numerical methods is about 3%. However,

this error margin widens to approximately 8% when the tunnel length decreases to 160 m (a ratio of 1:12) or increases to 220 m (a ratio of 1:9).

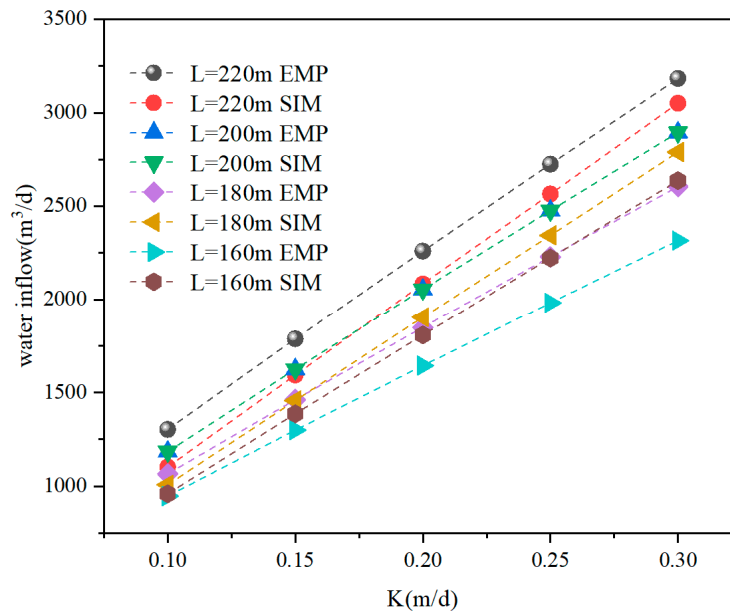


Figure 4. Comparison chart of empirical formula method and model method for calculating water inflow with different permeability coefficients.

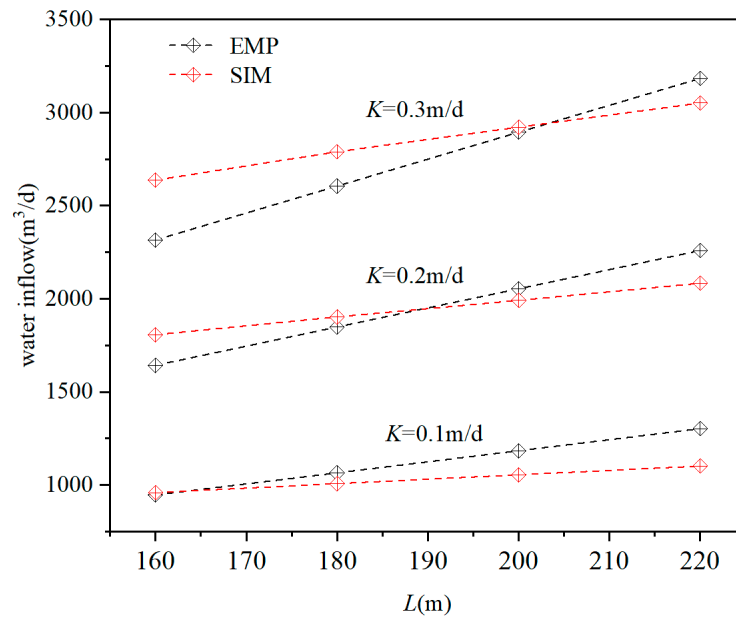


Figure 5. Comparison chart of empirical formula method and model method for calculating water inflow with different tunnel lengths.

The analysis reveals that with a fixed permeability coefficient and shorter tunnel lengths, the model’s water inflow estimates are higher than the empirical method’s average. Yet, as tunnel length extends, the model-generated water inflow gradually falls below the empirical formula’s calculations. Moreover, the point at which both methods yield identical water inflow estimates shifts to longer tunnel lengths as the subsoil’s permeability coefficient increases.

4. Engineering Case Study

The new value method introduced in this paper proves effective, showcasing minimal errors in ideal calculation scenarios and high precision in forecasting tunnel water inrush under perfect conditions. Such promising outcomes establish a solid basis for applying this method to real-world projects, allowing its practical usefulness and flexibility to be thoroughly assessed. Next, we will detail the application of this method in actual engineering projects.

4.1. Project Introduction

The Central Yunnan Water Diversion Project plays a crucial role in utilizing water from the Jinsha River, employing water pumping stations for extraction. Specifically designed as a first-level underground station, it is nestled in the mountains along the right bank of the Chongjiang River. The project draws water approximately 1.5 km upstream from Shigu, directing it through a 1.27 km detour channel, then via a 3.0 km tunnel and a 0.8 km culvert to an underground pump above Zhuyuan Village. From there, water ascends to the Xianglushan Tunnel entrance, traversing pipelines ranging from 4563.58 m to 4337.40 m in length.

The station's bedrock comprises primarily limestone and marble interspersed with shale, notably within the first section of the Qiongcuo Formation (D2q1) and the fourth section of the Ranjiawan Formation (D1r4). Quaternary deposits along the Chongjiang riverbed and adjacent gentle slopes are predominantly alluvial, with the riverbed's composition featuring gravel, pebbles, alluvium, clay and silty soil lenses, measuring 129–132.8 m in thickness.

4.2. Instance Model Parameter Settings

The study area, covering 6.7 km², is bordered by the Chongjiang River to the north and by the surface secondary watershed to the east and south, as illustrated in Figure 6. The model's northwest boundary aligns with the Chongjiang River, marked by a head value of 1835 m, while the east and south boundaries follow the surface watershed. Atmospheric precipitation infiltrates the area's upper submerged surface, serving as the recharge boundary. Meanwhile, the lower boundary, positioned at an elevation of 1660 m, functions as the isolation boundary.

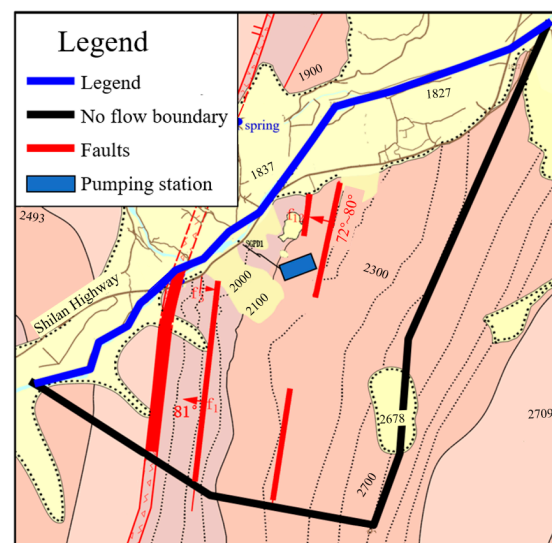


Figure 6. Shigu water source underground pumping room area and numerical simulation model boundary type.

Based on existing borehole data, a hydrogeological structural model of the study area was developed, as shown in Figure 7. Comparing this model and its profile with the actual

geological profile indicates that the structural model effectively and accurately reflects the regional stratigraphic distribution. Thus, it provides a solid foundation for constructing the subsequent three-dimensional infiltration model.

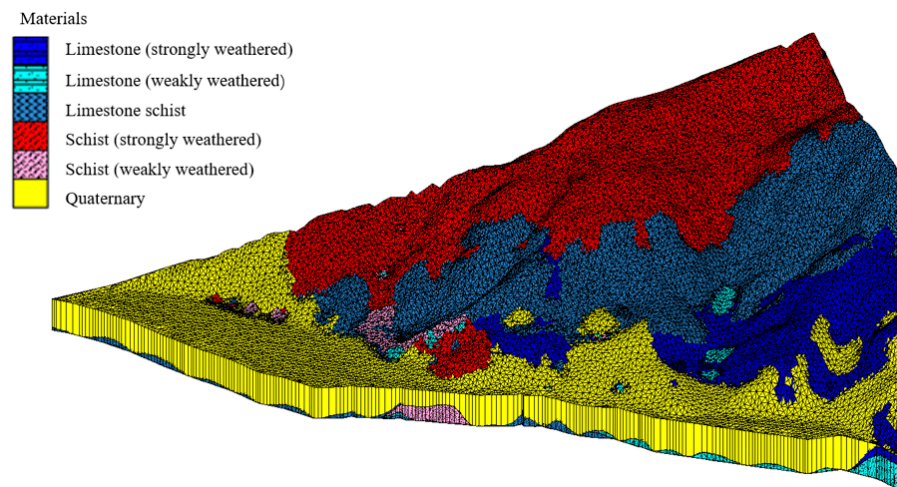


Figure 7. Shigu water source underground pumping room numerical simulation 3D geological structure model.

The rock's permeability coefficient is determined from pressurized water and oscillation test results. Since these tests are conducted below the groundwater table, they mainly reveal the water-bearing rock's permeability within the drill section. For the rock material's permeability in the unsaturated zone or areas not reached by drilling, analogy and inversion methods are employed for estimation. These borehole tests assess the permeability of rock masses at specific depths. Utilizing data from on-site pressurized water and micro-water tests, along with trial and error and numerical inversion techniques, we evaluated the underground water source at Shigu. The permeability coefficients of different lithologies in the pumping station model are shown in Table 3.

Table 3. Generalized types of lithology and corresponding aquifer permeability coefficients.

Lithology	K_x (cm/s)	K_x/K_y	K_x/K_z
Limestone (strongly weathered)	1.4×10^{-3}	1	3
Limestone (weakly weathered)	6.95×10^{-4}	1	3
Limestone schist	3.5×10^{-4}	1	3
Schist (strongly weathered)	1.16×10^{-5}	1	1
Schist (weakly weathered)	1.16×10^{-6}	1	1
Quaternary	1.16×10^{-2}	1	2

4.3. Model Calibration

By fine-tuning the model parameters, we aligned the actual water levels in the observation wells with those predicted by the model. Assessing the model's accuracy involved comparing the dynamic changes and observed water levels to see if they matched and if the fitted parameters reflected the true hydrogeological conditions.

From April 2016 to August 2017, nine boreholes in the Shigu Water Source Underground Pumping Station's main cavern area were under continuous groundwater level monitoring. During this time, groundwater levels were mostly stable, showing variations of around 10 m, though some boreholes experienced more significant fluctuations, with differences of up to 22 m. The model was refined using 17 selected water level values from the groundwater isopotential map provided to the contractors. The fitting results for each borehole are displayed in Figure 8. Despite limited water level data in the area,

the calculation error for water levels remained under 20 m, satisfying the requirements for accuracy.

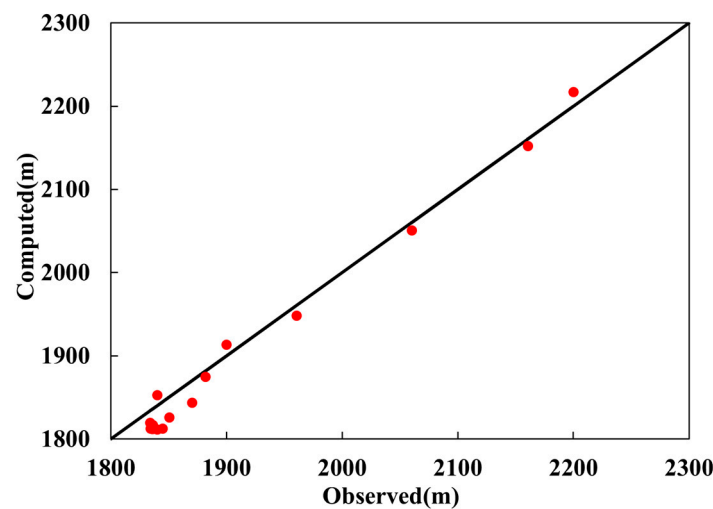


Figure 8. Comparison chart of observed water levels at observation holes and model simulated water levels in the study area.

4.4. Water Inflow Prediction Results

From the engineering geology map of the site, the diameters of the main pump room, the main transformer well and the water outlet maintenance valve room are 23.4 m, 15.0 m and 9.6 m, respectively. According to the Formula (9), the value of the discharge coefficient (C) in the chamber can then be determined for each hole and the water inflow volume in each cavern can be calculated (Table 4).

Table 4. Statistical table of water inflow in each cavern.

Engineering Parts	C (m ² /d)	Elevation of Water Outlet Point (m)	Water Inflow Date	Water Inflow (m ³ /d)	Forecast Water Inflow (m ³ /d)
Main room	5.51	1794.5	21.6–21.9	1440	1436.54
Traffic room	3.53	1800.4	21.9	1680	1005.95
Outlet room	2.26	1765	21.10–21.11	1200	1445.17

A comparison of actual vs. simulated water inflow volumes for each cavern in the underground pumping station is illustrated in Figure 9. The lowest simulation error, at 0.2%, occurs in the main pumping room. Conversely, the highest error, at 40.1%, is found in the main transformer traffic tunnel, leading to an average error across the three caverns of 20.2%.

The differences between observed and simulated water inflow volumes stem from key factors:

Model Simplifications: Despite its complexity, the numerical model simplifies certain physical processes. Notably, it cannot precisely capture the anisotropy of the aquifer surrounding the tunnel.

Temporal Dynamics: The model does not fully consider changes in hydraulic head caused by seasonal rainfall or other external influences. This oversight in the steady flow model can result in inaccuracies.

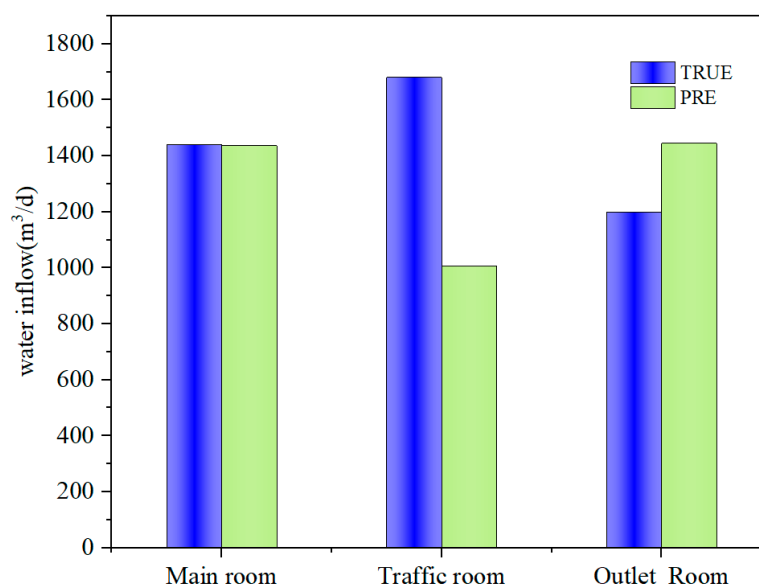


Figure 9. Comparison chart of water inflow in each cavern.

5. Conclusions

Accurately predicting tunnel water inflow is crucial for construction progress and structural safety. Numerical simulation methods are particularly beneficial in contexts with complex geological settings and irregular boundary conditions. This article leverages the Groundwater Model System (GMS) simulation software to evaluate the effectiveness, precision and practicality of employing the DRAIN module for delineating tunnel boundaries and calculating water inflow.

- (1) The article delineates the physical significance and valuation method for key parameters within the DRAIN module, highlighting its accuracy in estimating water inflow volumes for typical drop tunnels. The drainage coefficient (C) value, tied to the permeability coefficient of the surrounding rock and the influence area's definition, is calculable from the rock's thickness post-excavation, equating to twice the tunnel's radius. Ideally, the method's results should closely align with empirical formulas, with discrepancies not surpassing 10%.
- (2) Practical applications of the method yield promising outcomes, with the article outlining procedural steps and considerations for its application. It presents a swift, efficient and effective numerical approach for tunnel water inflow estimation, laying a solid foundation for seepage control and enhancing tunnel construction safety.

This method cannot be applied when the tunnel length is too large in proportion to the study area, and the method cannot be applied to transient flow. Future efforts should concentrate on creating a tool or guideline that dynamically adjusts simulation parameters across different tunnel geometries, expanding the method's relevance to a variety of designs. Moreover, incorporating transient flow simulations into groundwater models is essential for a temporal understanding of groundwater dynamics, including seasonal variances and potential climate change effects on water levels. These developments are expected to refine water inflow predictions and management within tunnel engineering.

Author Contributions: Z.C.: Conceptualization, Formal Analysis, Writing—Review and Editing, Visualization; Z.S.: Software, Formal Analysis, Investigation, Writing—Original Draft; M.L.: Software, Validation, Formal Analysis, Investigation; Q.S.: Conceptualization, Formal Analysis, Writing—Review and Editing, Visualization; L.F.: Resources and Software; Y.Z.: Conceptualization and Investigation. All authors have read and agreed to the published version of the manuscript.

Funding: This research was funded by Yunnan Provincial Department of Science and Technology: 202002AF080003; Jiangsu Provincial Natural Science Foundation General Project: No. BK20221507; Beijing Jiange Water Development Foundation: YC202308.

Data Availability Statement: Data is contained within the article.

Acknowledgments: The authors acknowledge valuable comments from the reviewers, which led to significant improvement of the paper.

Conflicts of Interest: Author Mei Li, Lufei Fan and Yanjie Zhang were employed by the company Dianzhong Water Diversion Co. The remaining authors declare that the research was conducted in the absence of any commercial or financial relationships that could be construed as a potential conflict of interest.

References

- Chen, J.; Zhang, W.; Ma, J.; Zeng, B.; Huang, Y. An analytical approach to study the reinforcement performance of rock anchors. *Eng. Fail. Anal.* **2024**, *160*, 108200. [\[CrossRef\]](#)
- Katibeh, H.; Aalianvari, A. Development of a New Method for Tunnel Site Rating from. *J. Appl. Sci.* **2009**, *9*, 1496–1502. [\[CrossRef\]](#)
- Zarei, H.; Uromeihy, A.; Sharifzadeh, M. A new tunnel inflow classification (TIC) system through sedimentary rock masses. *Tunn. Undergr. Space Technol.* **2013**, *34*, 1–12. [\[CrossRef\]](#)
- Hwang, J.-H.; Lu, C.-C. A semi-analytical method for analyzing the tunnel water inflow. *Tunn. Undergr. Space Technol.* **2007**, *22*, 39–46. [\[CrossRef\]](#)
- Kolymbas, D.; Wagner, P. Groundwater ingress to tunnels—the exact analytical solution. *Tunn. Undergr. Space Technol.* **2007**, *22*, 23–27. [\[CrossRef\]](#)
- Maréchal, J.-C.; Perrochet, P. New analytical solution for the study of hydraulic interaction between Alpine tunnels and groundwater. *Bull. Soc. Geol. Fr.* **2003**, *174*, 441–448. [\[CrossRef\]](#)
- Perrochet, P. A simple solution to tunnel or well discharge under constant drawdown. *Hydrogeol. J.* **2005**, *13*, 886–888. [\[CrossRef\]](#)
- Verruijt, A. A complex variable solution for a deforming circular tunnel in an elastic half-plane. *Int. J. Numer. Anal. Methods Geomech.* **1997**, *21*, 77–89. [\[CrossRef\]](#)
- Park, K.-H.; Owatsiriwong, A.; Lee, J.-G. Analytical solution for steady-state groundwater inflow into a drained circular tunnel in a semi-infinite aquifer: A revisit. *Tunn. Undergr. Space Technol.* **2008**, *23*, 206–209. [\[CrossRef\]](#)
- Gattinoni, P.; Scesi, L. An empirical equation for tunnel inflow assessment: Application to sedimentary rock masses. *Hydrogeol. J.* **2010**, *18*, 1797–1810. [\[CrossRef\]](#)
- Farhadian, H.; Nikvar Hassani, A.; Katibeh, H. Groundwater inflow assessment to Karaj Water Conveyance tunnel, northern Iran. *KSCCE J. Civ. Eng.* **2017**, *21*, 2429–2438. [\[CrossRef\]](#)
- Farhadian, H.; Katibeh, H.; Huggenberger, P.; Butscher, C. Optimum model extent for numerical simulation of tunnel inflow in fractured rock. *Tunn. Undergr. Space Technol.* **2016**, *60*, 21–29. [\[CrossRef\]](#)
- Farhadian, H.; Katibeh, H.; Huggenberger, P. Empirical model for estimating groundwater flow into tunnel in discontinuous rock masses. *Environ. Earth Sci.* **2016**, *75*, 471. [\[CrossRef\]](#)
- Shi, M.; Hu, W.; Li, M.; Zhang, J.; Song, X.; Sun, W. Ensemble regression based on polynomial regression-based decision tree and its application in the in-situ data of tunnel boring machine. *Mech. Syst. Signal Process.* **2023**, *188*, 110022. [\[CrossRef\]](#)
- Dai, Z.; Li, X.; Lan, B. Three-dimensional modeling of tsunami waves triggered by submarine landslides based on the smoothed particle hydrodynamics method. *J. Mar. Sci. Eng.* **2023**, *11*, 2015. [\[CrossRef\]](#)
- Tisler, W.; Szymkiewicz, A. Air trapping problem during infiltration on the large areas. In Proceedings of the 10th Conference on Interdisciplinary Problems in Environmental Protection and Engineering EKO-DOK 2018, Polanica-Zdrój, Poland, 16–18 April 2018.
- Guo, Y.F.; Wang, H.N.; Jiang, M.J. Efficient Iterative Analytical Model for Underground Seepage around Multiple Tunnels in Semi-Infinite Saturated Media. *J. Eng. Mech.* **2021**, *147*, 04021101. [\[CrossRef\]](#)
- Zhang, K.; Xue, Y.G.; Xu, Z.H.; Su, M.X.; Qiu, D.H.; Li, Z.Q. Numerical study of water inflow into tunnels in stratified rock masses with a dual permeability model. *Environ. Earth Sci.* **2021**, *80*, 260. [\[CrossRef\]](#)
- Zhao, X.; Yang, X.H. Experimental study on water inflow characteristics of tunnel in the fault fracture zone. *Arab. J. Geosci.* **2019**, *12*. [\[CrossRef\]](#)
- Tong, S.; Dong, Y.; Wang, L. Methods and applications of an unstructured grid version of MODFLOW: MODFLOW-USG. *Hydrogeol. Eng. Geol.* **2016**, *43*, 9–16.
- Ju, Q.; Hao, Z.; Yu, Z.; Chen, X.; She, C. Study of the Model of Spring Flow Forecast A Case Study of the Xiaonanhai Spring Catchment. *J. Sichuan Univ. Eng. Sci. Ed.* **2011**, *43*, 77–82.
- Qingyong, W.; Zhonghua, J.I.A.; Xiaofeng, L.I.U.; Feng, S.H.I. Visual MODFLOW and its application to groundwater simulation. *J. Water Resour. Water Eng.* **2007**, *18*, 90–92.
- Xia, Q. Characteristics of Error in Numerical Modeling of Well Flow with MODFLOW. *Geotech. Investig. Surv.* **2007**, *37*, 29–32.
- Reimann, T. MODFLOW-2005 CFP—A hybrid model for karst aquifers. *Grundwasser* **2009**, *14*, 139–145. [\[CrossRef\]](#)

25. Zhang, B.; Hong, M.; Zou, Z.H.; Yeh, T.C.J.; Cheng, P. Embedding isochronous cells overland flow module into MODFLOW. *Hydrol. Process.* **2013**, *27*, 3833–3841. [[CrossRef](#)]
26. Cheng, T.P.; Shao, J.L.; Cui, Y.L.; Mo, Z.Y.; Han, Z.; Li, L. Parallel simulation of groundwater flow in the North China Plain. *J. Earth Sci.* **2014**, *25*, 1059–1066. [[CrossRef](#)]
27. Zhao, S.; Sun, S. Application of MODFLOW in Simulating Groundwater Seepage Flowing Field of Tiantai Landslide in Sichuan Province. *J. Catastrophol.* **2007**, *22*, 50–53.
28. Raheem, A.; Ahmad, I.; Arshad, A.; Liu, J.P.; Rehman, Z.U.; Shafeeqe, M.; Rahman, M.M.; Saifullah, M.; Iqbal, U. Numerical Modeling of Groundwater Dynamics and Management Strategies for the Sustainable Groundwater Development in Water-Scarce Agricultural Region of Punjab, Pakistan. *Water* **2024**, *16*, 34. [[CrossRef](#)]
29. Sanaullah, M.; Wang, X.Q.; Ahmad, S.R.; Mirza, K.; Mahmood, M.Q.; Kamran, M. Optimized Irrigated Water Management Using Numerical Flow Modeling Coupled with Finite Element Model: A Case Study of Rechna Doab, Pakistan. *Water* **2023**, *15*, 4193. [[CrossRef](#)]
30. Rubio-Arellano, A.B.; Ramos-Leal, J.A.; Vázquez-Báez, V.M.; Mora, J.I.R. Modeling the Groundwater Dynamics of the Celaya Valley Aquifer. *Water* **2023**, *15*, 1. [[CrossRef](#)]
31. Li, W.; Zhang, B.; Hong, M.; Wang, B. Application of Visual MODFLOW in Assessment of Groundwater Resources in Longxi Area of Daqing. *World Geol.* **2003**, *22*, 161–165.
32. Diaz, M.; Sinicyn, G.; Grodzka-Lukaszewska, M. Modelling of Groundwater-Surface Water Interaction Applying the Hyporheic Flux Model. *Water* **2020**, *12*, 3303. [[CrossRef](#)]
33. Ostad, H.; Mohammadi, Z.; Fiorillo, F. Assessing the Effect of Conduit Pattern and Type of Recharge on the Karst Spring Hydrograph: A Synthetic Modeling Approach. *Water* **2023**, *15*, 1594. [[CrossRef](#)]
34. Hunt, M.; Marandi, A.; Retike, I. Water Balance Calculation for a Transboundary Aquifer System between Estonia and Latvia. *Water* **2023**, *15*, 3327. [[CrossRef](#)]
35. Xu, H.; Li, G.; Dong, Y.; Zhang, S.; Li, M. An approach for simulating planar flux based on MODFLOW. *Geotech. Investig. Surv.* **2011**, *39*, 37–39.
36. Wei, Y.; Xu, M.; Liu, J. Visual Modflow software and analysis on its application potential in study hydrogeological conditions of metallogenesis of sandstone-type uranium deposits. *Uranium Geol.* **2003**, *19*, 53–57.
37. Cheng, J. Analysis on Differences among Solutions by Different Equations in MODFLOW. *Geotech. Investig.* **2002**, *32*, 25–27.
38. Dong, P.; Wang, X. Application and discussion of MODFLOW's simulation to the seepage of free surface. *Geotech. Investig. Surv.* **2009**, *37*, 27–30.
39. Ma, C.; Li, K.; Shi, L.; Zhao, S.; Xia, Z. Application of visual modflow in simulation of an opencast mine underground water. *Environ. Eng.* **2011**, *29*, 98–101.
40. Shu, L.; Xu, Y.; Wu, P. Groundwater Flow Numeric Simulation Method Based on Uncertainties of MODFLOW Parameters. *J. Jilin Univ. Earth Sci. Ed.* **2017**, *47*, 1803–1809.
41. Qin, J.; Du, T.Z.; Hao, Z.C.; Xu, H.Q.; Li, B.T. Integration of artificial neural networks with a numerical groundwater model for simulating spring discharge. In Proceedings of the Advances in Energy Science and Equipment Engineering, Guangzhou, China, 30–31 May 2015; pp. 1197–1201.
42. Liu, D.; Si, G.; Zheng, J.; Yu, J.; Liu, Y.; Chen, J.; Ma, J. Numerical Simulation and Impact Assessment of a Groundwater Pollution Based on MODFLOW. *Radiat. Prot.* **2013**, *33*, 30–36.
43. Batelaan, O.; De Smedt, F. SEEPAGE, a new MODFLOW DRAIN package. *Ground Water* **2004**, *42*, 576–588. [[CrossRef](#)] [[PubMed](#)]
44. Rodriguez, L.B.; Cello, P.A.; Vionnet, C.A.; Goodrich, D. Fully conservative coupling of HEC-RAS with MODFLOW to simulate stream—Aquifer interactions in a drainage basin. *J. Hydrol.* **2008**, *353*, 129–142. [[CrossRef](#)]
45. Golian, M.; Teshnizi, E.S.; Nakhaei, M. Prediction of water inflow to mechanized tunnels during tunnel-boring-machine advance using numerical simulation. *Hydrogeol. J.* **2018**, *26*, 2827–2851. [[CrossRef](#)]
46. Sartirana, D.; Zanolli, C.; Rotiroli, M.; De Amicis, M.; Caschetto, M.; Redaelli, A.; Fumagalli, L.; Bonomi, T. Quantifying Groundwater Infiltrations into Subway Lines and Underground Car Parks Using MODFLOW-USG. *Water* **2022**, *14*, 4130. [[CrossRef](#)]
47. Zhao, L.; Xia, R.; Yang, Y.; Shao, J.; Yi, L.; Wang, Z. Discussion and application of simulation methods for karst conduit flow based on MODFLOW. *Carsologica Sin.* **2017**, *36*, 346–351. [[CrossRef](#)]
48. Bredihin, V.V.; Akulshin, A.A.; Vladimirovna, B.N.; Sergeevna, P.V. A method of calculating filtration rate of an infiltration water intake in kursk region. *J. Appl. Eng. Sci.* **2017**, *15*, 208–211. [[CrossRef](#)]
49. Wu, J.; Zhou, Z.; Li, M.; Chen, M. Advance on the methods for predicting water inflow into tunnels. *J. Eng. Geol.* **2019**, *27*, 890–902. [[CrossRef](#)]

Disclaimer/Publisher's Note: The statements, opinions and data contained in all publications are solely those of the individual author(s) and contributor(s) and not of MDPI and/or the editor(s). MDPI and/or the editor(s) disclaim responsibility for any injury to people or property resulting from any ideas, methods, instructions or products referred to in the content.